

# Ultrathin NiOOH Nanosheets Directly Assembled on Reduced Graphene Oxide Surface as Electrocatalyst for Oxidation of Glucose and Reduced Glutathione

Su-Juan Li<sup>\*</sup>, Wei Guo, Rui-Ting Liu, Ji-Min Du

Henan Province Key Laboratory of New Optoelectronic Functional Materials, College of Chemistry and Chemical Engineering, Anyang Normal University, Anyang, 455000, Henan, China.

\*E-mail: [lemontree88@163.com](mailto:lemontree88@163.com)

Received: 27 May 2016 / Accepted: 11 July 2016 / Published: 7 August 2016

---

The aqueous NiOOH with ultrathin nanosheets structure were prepared using a hydrothermal strategy and characterized by atomic force microscopy (AFM), X-ray diffraction (XRD) and scanning electron microscopy (SEM). It was modified on electrochemically reduced graphene oxide electrode through a self-assembly method to form NiOOH/RGO nanocomposites electrode. SEM, energy-dispersive X-ray analysis and electrochemical impedance spectroscopy were employed to characterize the resultant NiOOH/RGO nanocomposites electrode. To study the electrocatalytic properties of the NiOOH/RGO nanocomposites, glucose and reduced glutathione (GSH) were selected as model small molecules. An favorable electrocatalytic activities of the NiOOH/RGO electrode was obtained toward oxidation of glucose and GSH. The present NiOOH/RGO nanocomposites based amperometric sensor showed a rapid and highly sensitive response to glucose and GSH, which might find promising applications in medical applications, biological fuel cells and diseases diagnosis.

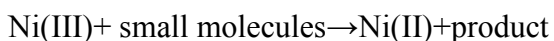
---

**Keywords:** Nickel oxide hydroxide nanosheets; Reduced graphene oxide; Electrocatalyst; Glucose; Reduced glutathione

## 1. INTRODUCTION

Recently, electrocatalysis toward small molecules using different types of materials with designed morphology has aroused extensive and increased attention due to its potential applications in technological fields of sensors and biosensors [1,2], energy conversion devices [3], fuel cells [4,5] and electrocatalysis [6,7]. The materials used as electrochemical catalysts include various metals such as Pt, Au, Ag, Mn, Ni, Cu, Co etc. and their oxides or hydroxides [6-11]. Among those materials, nickel based electrocatalysts have arisen much research interest and become the subject of much investigation

because of their high electrocatalytic activity, good stability, low cost and the high natural abundance. A wide range of small molecules, such as glucose [12,13], ethanol [14], glycine [15], dopamine [16], H<sub>2</sub>O<sub>2</sub> [17], and chlorophenol [18] et al. have been reported for enhanced oxidation performance at the Ni based electrocatalysts. Ni<sup>2+</sup>/Ni<sup>3+</sup> redox couple mediated electrocatalysis is commonly employed to illustrate the mechanism of these Ni based materials like Ni, NiO and NiOOH toward electrooxidation of organic small molecules [9,19-21]. As shown in the below equations, Ni based electrocatalysts are firstly transformed to Ni(III) in alkaline solution at a given potential, and then Ni(III) strongly adsorbs small organic substances and subsequently induces their oxidation and it in turn gets reduced back to divalent nickel, achieving electrocatalytic cycles.



Apart from the redox properties, the structure of the Ni based electrocatalyst is also important as it can affect the electrocatalytic activities of the materials. Recent investigations found that electrodes modified with well-defined nanostructures are likely to have improved electrochemical behavior and performance, due to the large surface area and improved mass and electron transport of electrolytes at the electrode–electrolyte interface. In particular, regularly ordered Ni based nanostructures, such as nanofoam [20], nanoribbons [22], nanoplates [23], nanoflake [24], nanoparticles [19], nanowires [25], nanospheres [12,26], and nanosheets [13] have been demonstrated to enhance electron transport, leading to excellent electrochemical performances. Moreover, to further enhance the catalytic performance of the Ni based materials, an effective method is loaded it on various carbon materials support. Graphene, a promising carbon material, is anticipated to have great potential as catalysts support and promoter thanks to its unique sheet morphology, ultrahigh electron conductivity, and high surface area [27,28]. Zhang et al. prepared a novel reduced graphene oxide (RGO)-NiOOH nanocomposite with monodispersed NiOOH nanoplates assembled on RGO nanosheets and applied this two dimensional nanocomposite for enzyme-free glucose sensing [23]. Lu et al. fabricated a novel composite film of nickel oxide hollow spheres–RGO–nafion modified glassy carbon electrode and applied in the sensitive and selective determination of glucose [29]. Gao et al. developed NiOOH/electroreduced graphene oxide (ERGO)–MWNT nanocomposites via a convenient electrodeposition method and demonstrated its use in glucose and H<sub>2</sub>O<sub>2</sub> sensing [30]. These findings inspired us to fabricate high performance of graphene loaded Ni based electrocatalyst and explore its potential application for enhanced electrocatalytic activity toward oxidation of small organic molecules.

Inspired by this, we synthesized aqueous NiOOH nanosheets with ultrathin structure via a hydrothermal method. Self-assembly technique was used to assemble the obtained NiOOH nanosheets onto the surface of two-dimensional RGO which was pre-prepared on glassy carbon electrode by electrodeposition method. The physical adsorption and electrostatic interaction are believed to contribute to the direct assembly of NiOOH nanosheets on RGO surface, without the aid of any poorly conductive polymers as linkers. To evaluate the electrocatalytic properties of the resultant NiOOH/RGO nanocomposites electrode, glucose and reduced glutathione (GSH) were selected as model small organic molecules due to their biological importance especially in functions of blood glucose detection and antioxidant defense respectively. An excellent performance of the developed

NiOOH/RGO electrode in terms of wide linear range, high sensitivity and selectivity, good stability was obtained for sensing of glucose and GSH.

## 2. EXPERIMENTAL SECTION

### 2.1. Reagents and apparatus

GO was obtained from Nanjing XFNANO Materials Tech Co., Ltd. Glucose, GSH, ascorbic acid, dopamine, uric acid, fructose, lactose and polyvinyl pyrrolidone (PVP) and nickel acetate were purchased from Sigma Aldrich. The supporting electrolyte was prepared from the salts  $\text{Na}_2\text{HPO}_4$  and  $\text{KH}_2\text{PO}_4$  to a 0.1 M phosphate buffer solution (PBS, pH 7.0). Ultrapure water (18.2 M $\Omega$  cm) produced by a Milli-Q system was used as the solvent throughout the whole work.

SEM and energy dispersive X-ray spectroscopy (EDS) was characterized by a Hitachi SU-8010 field-emission scanning electron microscope (Japan). AFM images of the obtained NiOOH was performed on a Dimension Edge microscope (Bruker Nano Inc., Santa Barbara, CA) equipped with a tapping mode. Microstructures of the product were characterized by X-ray diffraction (XRD, Rigaku Ultima III) with a Cu K $\alpha$  ( $\lambda = 1.5418 \text{ \AA}$ ). Electrochemical related experiments were obtained by a CHI 660D electrochemical station (Shanghai, China) with a conventional three-electrode system, where the NiOOH/RGO nanocomposites electrode served as the working electrode, a platinum wire as the counter electrode and a saturated calomel electrode (SCE) as the reference electrode.

### 2.2. Synthesis of NiOOH nanosheets aqueous solution

Typically, 0.0003 mol of  $\text{Ni}(\text{Ac})_2$  and 0.002 mol of urea were dissolved in 50 mL of distilled water, then 0.1 g PVP was added. The obtained solution was magnetically stirred for 30 min at room temperature and then transferred into a Teflon-lined stainless steel autoclave. Afterwards the autoclave was sealed and maintained at 100 °C for 24 h, and subsequently allowed to cool to room temperature naturally. The resulting products were collected and washed three times with water and ethanol. Then, it was dispersed in water for a concentration of 5 mg/mL.

### 2.3. Assembly of NiOOH nanosheets on RGO modified glassy carbon electrode

Prior to modification, the GC electrode was pretreated to a mirror-like surface using 0.3 and 0.05  $\mu\text{m}$  alumina slurries sequentially, and then ultrasonically cleaned in water. A 10  $\mu\text{L}$  portion of 1 mg mL $^{-1}$  GO aqueous dispersion was dripped onto the polished glassy carbon electrode (GCE), after drying at room temperature, the GO modified GCE (GO/GCE) was obtained. Then, the GO/GCE was immersed into 0.1 M  $\text{KH}_2\text{PO}_4$  solution, and a applied potential of -1.5 V was kept for 10 min by using potentiostat. The as-prepared RGO/GCE was immersed into the obtained NiOOH aqueous dispersion for 2 hour to achieve a saturated adsorption through self-assembly method driven by the physical and electrostatic interaction, thus, a resulting NiOOH/RGO/GCE was obtained. After that, the electrode

was rinsed with ultrapure water. For contrast, NiOOH/GCE was prepared by directly dipping bare GCE into the obtained NiOOH aqueous dispersion for 2 hour.

### 3. RESULTS AND DISCUSSION

#### 3.1. Morphological characterizations

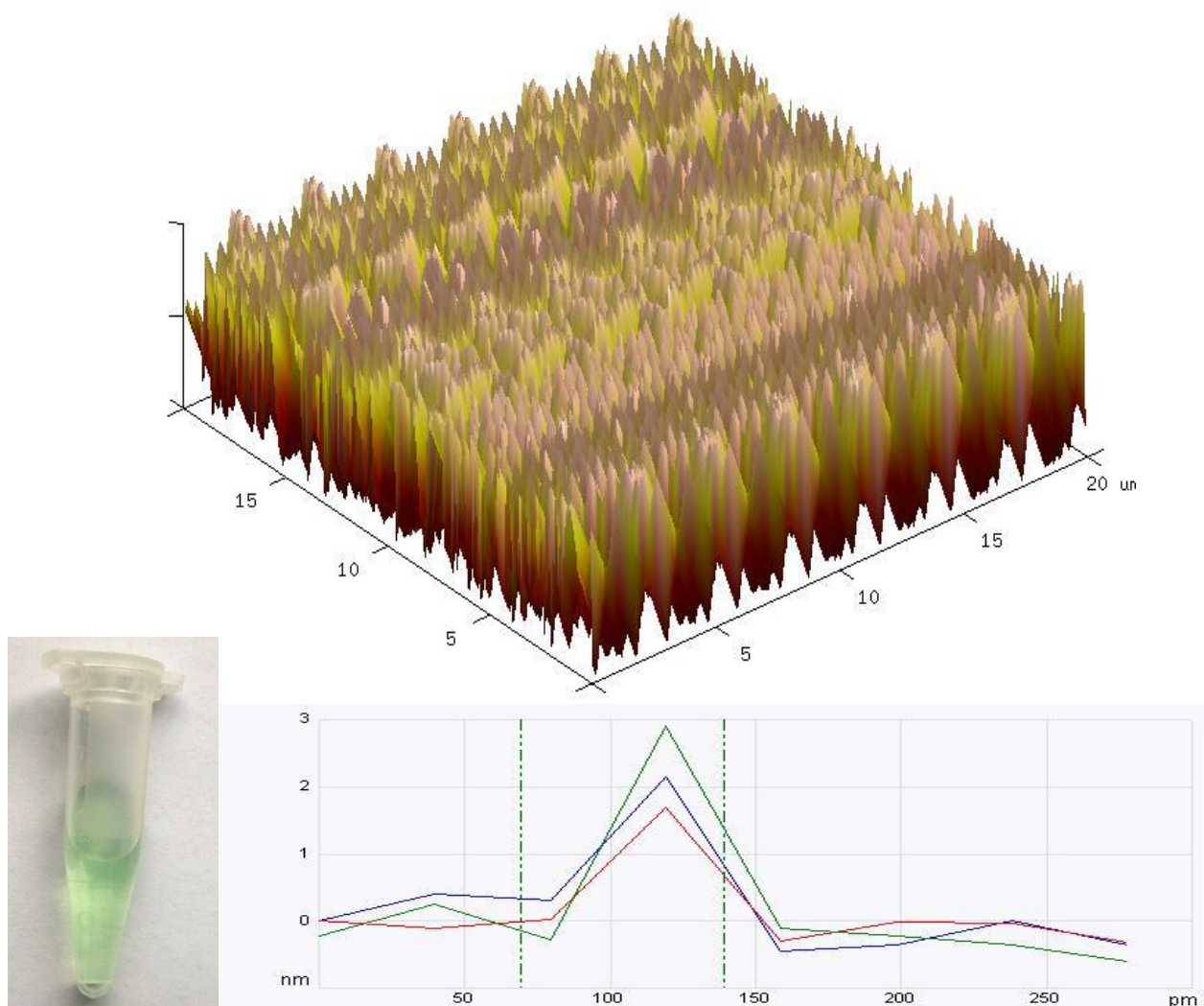


**Figure 1.** Three-dimensional AFM image of the obtained NiOOH dispersing on a mica slice with the measurement curve for typical three nanosheets, and the optical photograph of NiOOH aqueous solution displayed in bottom left.

Fig. 1 shows the three-dimensional AFM image of NiOOH dispersed on a mica slice. A large number of flake-like NiOOH nanosheets are observed. From the corresponding measurement curve for three typical nanosheets, horizontal axis is related to the thickness of NiOOH nanosheets and the vertical axis is corresponds to the height of nanosheets. Obviously, the thickness of NiOOH nanosheets is homogenous with size of about 0.1 nm, which is much smaller that (10 nm thickness) of reported 3D porous NiO nanosheets synthesized by chemical bath deposition via a surfactant template [13]. This

ultrathin flake-like shape makes the obtained NiOOH well-dispersed in aqueous solution to form a transparent green solution, as displayed in the optical photograph (bottom left in Fig. 1). This morphology of NiOOH nanosheets are characterized with a large surface area and rapid electron transport rate, which is special desirable for electrocatalytic applications. The crystal structure of the as-synthesized NiOOH nanosheets was confirmed by XRD technique and the diffraction patterns are shown in Fig. 2. Obviously, the diffraction patterns show a good agreement with the main peaks of the standard diagram (JCPDS card NO: 06-0075). The well-defined two strong diffraction peaks are located approximately  $2\theta$  values of  $12.7^\circ$ ,  $25.9^\circ$  and  $59.5^\circ$  which corresponds to the (003) and (006) planes of the crystal structure of NiOOH nanosheets, respectively. Other insignificant diffraction peaks belongs to the (101), (102), (104), (108), (110) planes of NiOOH nanosheets.

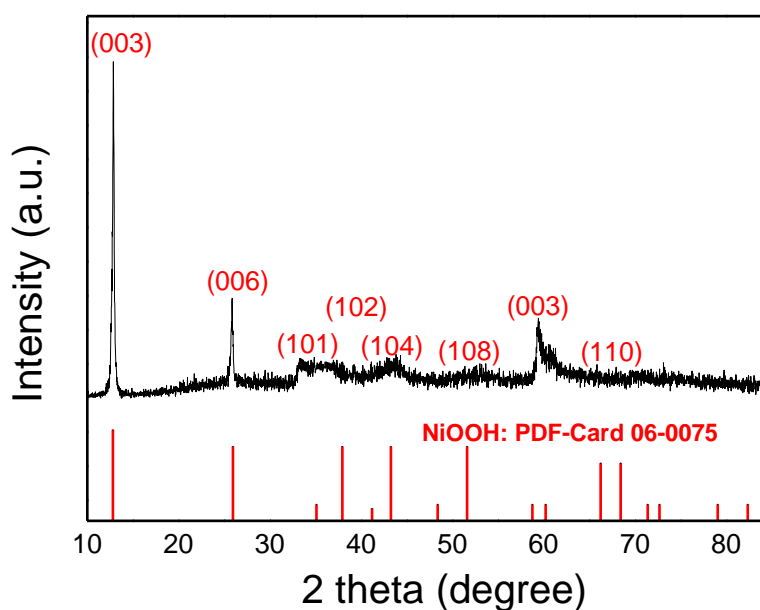


**Figure 2.** XRD patterns of the as- synthesized NiOOH nanosheets.

Fig. 3a shows the high-resolution SEM image of the obtained NiOOH dispersed on Si slice. NiOOH nanosheets with plenty of stacking and scrolling are observed, the shape of which can provide large surface area. The electrochemically prepared RGO/GCE (Fig. 3b) displays the typical characteristics of graphene with wrinkled structures [31,32]. After the RGO/GCE was modified with NiOOH nanosheets through a self-assembled method to form NiOOH/RGO electrode, the structure of NiOOH nanosheets with plenty of stacking and scrolling is also observed, as shown in Fig. 3c, which demonstrates that the NiOOH nanosheets have been successfully assembled on RGO surface. The EDX mapping image of NiOOH/RGO/GCE, as demonstrated in Fig. 3d, shows that the element of C, O and Ni could be observed, which further indicates the formation of NiOOH/RGO nanocomposites.

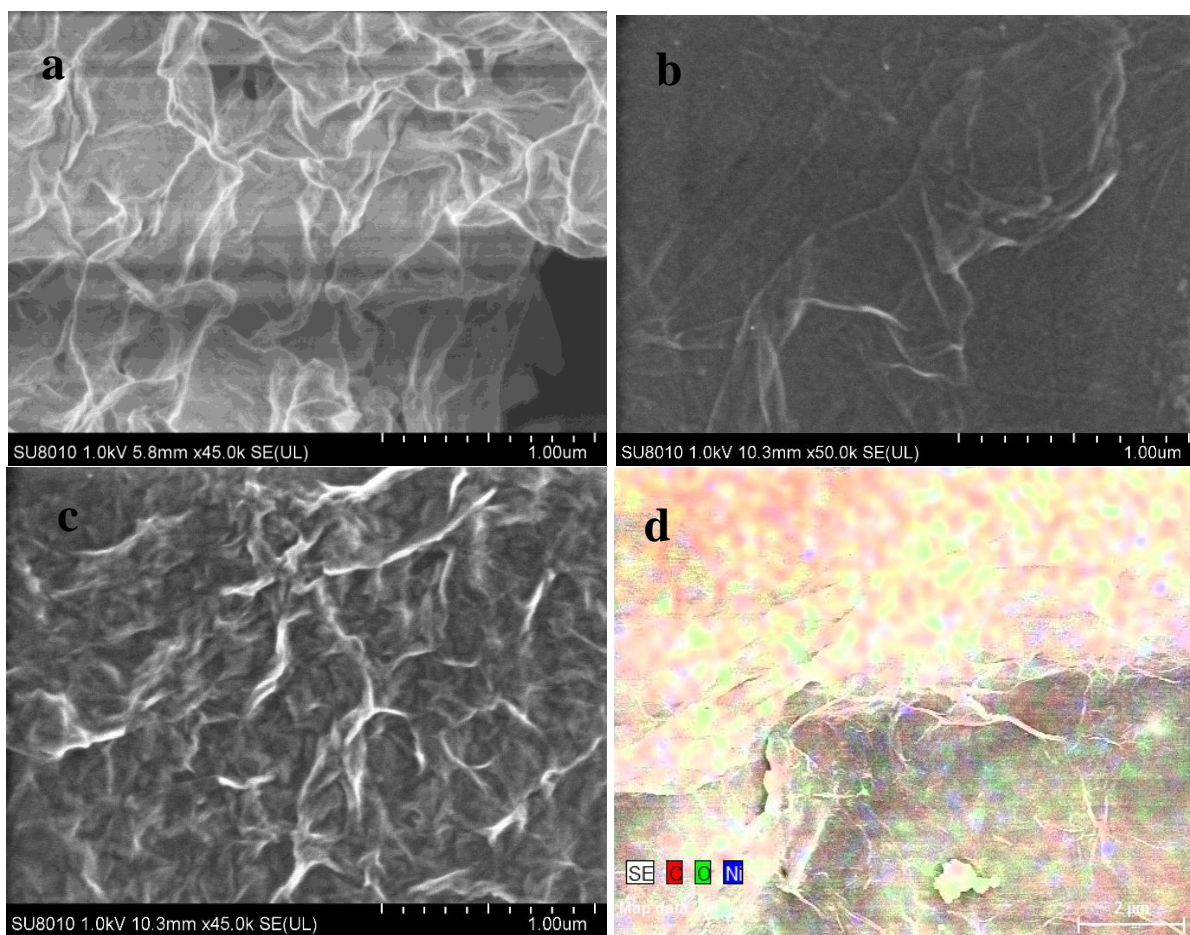


**Figure 3.** The SEM images of the obtained NiOOH dispersed on Si slice (a), RGO/GCE (b) and the NiOOH/RGO/GCE (c). (d) The EDX mapping image of NiOOH/RGO/GCE.

### 3.2. Electrochemical characterizations

Electrochemical impedance spectroscopic (EIS) measurements in 10 mM  $\text{Fe}(\text{CN})_6^{3-}/\text{Fe}(\text{CN})_6^{4-}$  and 0.1 M KCl were carried out to study the electron transfer behavior of the RGO supported NiOOH nanocomposites modified electrode. As shown in Fig. 4, after being modified with RGO nanosheets, the diameter of the semicircle, which relates to the charge transfer resistance ( $R_{ct}$ ) of the RGO/GCE was significantly decreased or nearly disappeared compared with the bare GCE, suggesting the excellent conductivity of RGO and its fast electron transfer rate. That's one of reasons that RGO was selected to support NiOOH nanosheets. The following adsorption of NiOOH nanosheets on RGO surface makes diameter of the semicircle larger than RGO/GCE, but still smaller than the bare GCE, due to RGO support promotes the charge transfer of NiOOH with comparatively low conductivity.

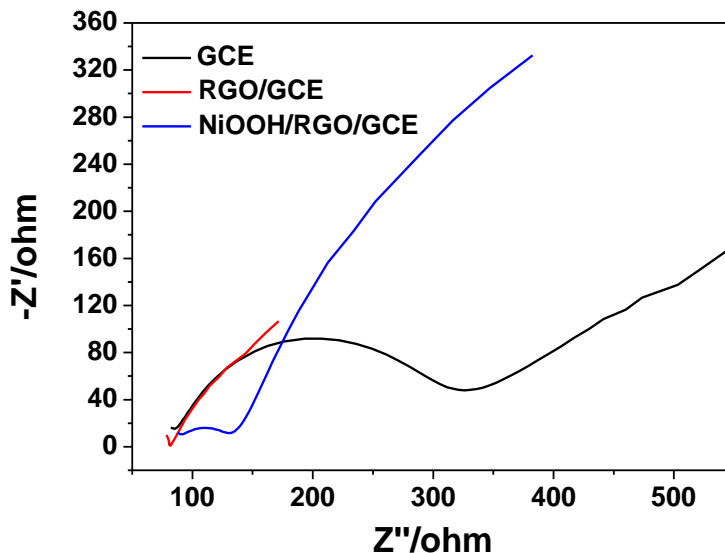


**Figure 4.** EIS plots measured in 10 mM  $[\text{Fe}(\text{CN})_6]^{3-/4-}$ +0.1 M KCl for the bare GCE, RGO/GCE and NiOOH/RGO/GCE. The frequency range of EIS was from 0.1 to  $10^5$  Hz at +0.2 V.

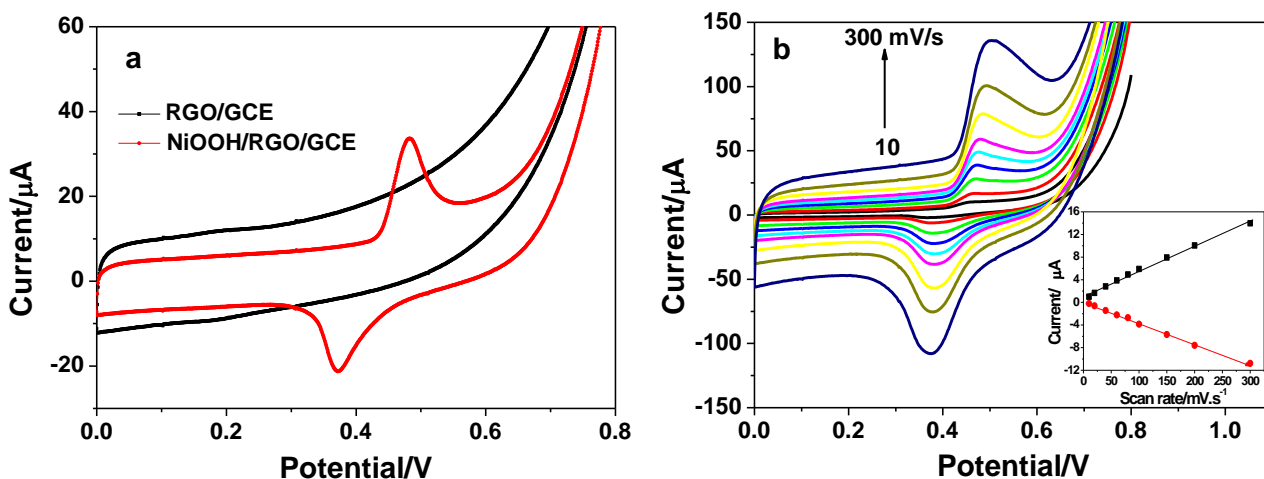


**Figure 5.** (a) CV responses of RGO/GCE and NiOOH/RGO/GCE in 0.1 M NaOH at scan rate of  $50 \text{ mV s}^{-1}$ ; (b) CV responses of NiOOH/RGO/GCE in 0.1 M NaOH at different scan rates (from inner to outer) of 10, 20, 40, 60, 80, 100, 150, 200,  $300 \text{ mV s}^{-1}$ .

To validate the successful immobilization of NiOOH nanosheets on RGO surface, the CV responses of NiOOH/RGO/GCE obtained in  $0.1 \text{ mol L}^{-1}$  NaOH are given in Fig. 5a. It can be seen that no redox peak was observed for RGO/GCE, indicating RGO was silent in the present potential range. However, an obvious redox peaks corresponding to  $\text{Ni}^{2+}/\text{Ni}^{3+}$  redox couple was obtained at NiOOH/RGO/GCE, indicating that the electrocatalyst of NiOOH nanosheets have been successfully assembled on RGO surface. The reaction kinetics of modified NiOOH on electrode surface was illustrated by investigation of CV responses of NiOOH/RGO/GCE at different scan rates. The results are shown in Fig. 5b. Obviously, the peak-to-peak separation ( $\Delta E_p$ ) became widened with increase of

scan rates. In the range of 10–300  $\text{mV s}^{-1}$ , both the oxidation and reduction peak currents are proportional to the scan rates (the linear relationship with correlation coefficients of 0.9967 and 0.9984 for oxidation and reduction peaks shown in the inset of Fig. 5b) respectively, suggesting that the electron transfer process in the NiOOH redox reaction takes place through a surface-controlled mechanism.

### 3.3. Electrocatalytic oxidation of glucose at the NiOOH/RGO nanocomposites electrode

Electrocatalysis toward the oxidation of glucose, a small molecule of scientific interest, is important not only to the development of novel blood glucose monitor devices but also application in other fields, such as the food monitoring, pharmaceutical analysis and the development of fuel cells and batteries [33-36]. Due to the limitations of enzymatic glucose systems, research interest in recent years has been focused on fabrication of novel materials as electrocatalyst for direct electrooxidation of glucose. The development of efficient non-enzymatic glucose sensors with rapid response, high detection sensitivity and stability, and excellent selectivity is the ultimate focus in analytical field.

Here, the direct electrocatalytic performance of the fabricated NiOOH/RGO nanocomposites electrode toward glucose oxidation was evaluated from its CV response in 0.1 M NaOH. In this respect, the RGO/GCE and NiOOH/GCE were used for comparison. Fig. 6 shows the CVs of different electrodes in 0.1 M NaOH solution without and with 5 mM of glucose involved at a scan rate of 50  $\text{mV s}^{-1}$ . As observed, the RGO/GCE (Fig. 6a) did not show distinct electrocatalysis toward oxidation of glucose in the scanned range of 0-0.8 V. After further modification of NiOOH nanosheets, a pair of redox peaks was obtained for NiOOH/RGO/GCE (Fig. 6b) in NaOH solution with an oxidation peak at 0.463 V and a reduction peak at 0.378 V (*vs* SCE), respectively, which was assigned to the  $\text{Ni(OH)}_2 + \text{OH}^- - \text{e}^- \rightarrow \text{NiOOH} + \text{H}_2\text{O}$  redox reaction [21,22]. Upon addition of glucose, due to fact that the added glucose was oxidized by NiOOH to gluconolactone ( $\text{NiOOH} + \text{glucose} \rightarrow \text{NiO} + \text{gluconolactone}$ ), an increase in oxidation current and a decrease in reduction current was observed, revealing direct electrocatalysis of  $\text{Ni}^{2+}/\text{Ni}^{3+}$  redox couple toward glucose oxidation following the above equations. However, the NiOOH/GCE showed indistinct redox peaks of  $\text{Ni}^{2+}/\text{Ni}^{3+}$  couple, probably arising from the small amount of NiOOH electrocatalyst loaded on bare GCE. The subsequent addition of glucose caused an identifiable increase in oxidation current from a potential of 0.5 V due to glucose oxidation catalyzed by the immobilized small amount of NiOOH nanosheets. These results indicate that the introduction of RGO remarkably facilitate the immobilization of NiOOH nanosheets on electrode surface and thus improve its electrocatalytic performance toward oxidation of glucose. The facile integration of NiOOH with RGO nanosheets by a self-assembly method resulted from four aspects: 1) the increased surface area and the oxygen-containing functional groups on RGO surface; 2) the driven force of electrostatic interactions and physical adsorption; 3) the favorable surface morphology due to easy combination between NiOOH nanosheet and RGO nanosheet.

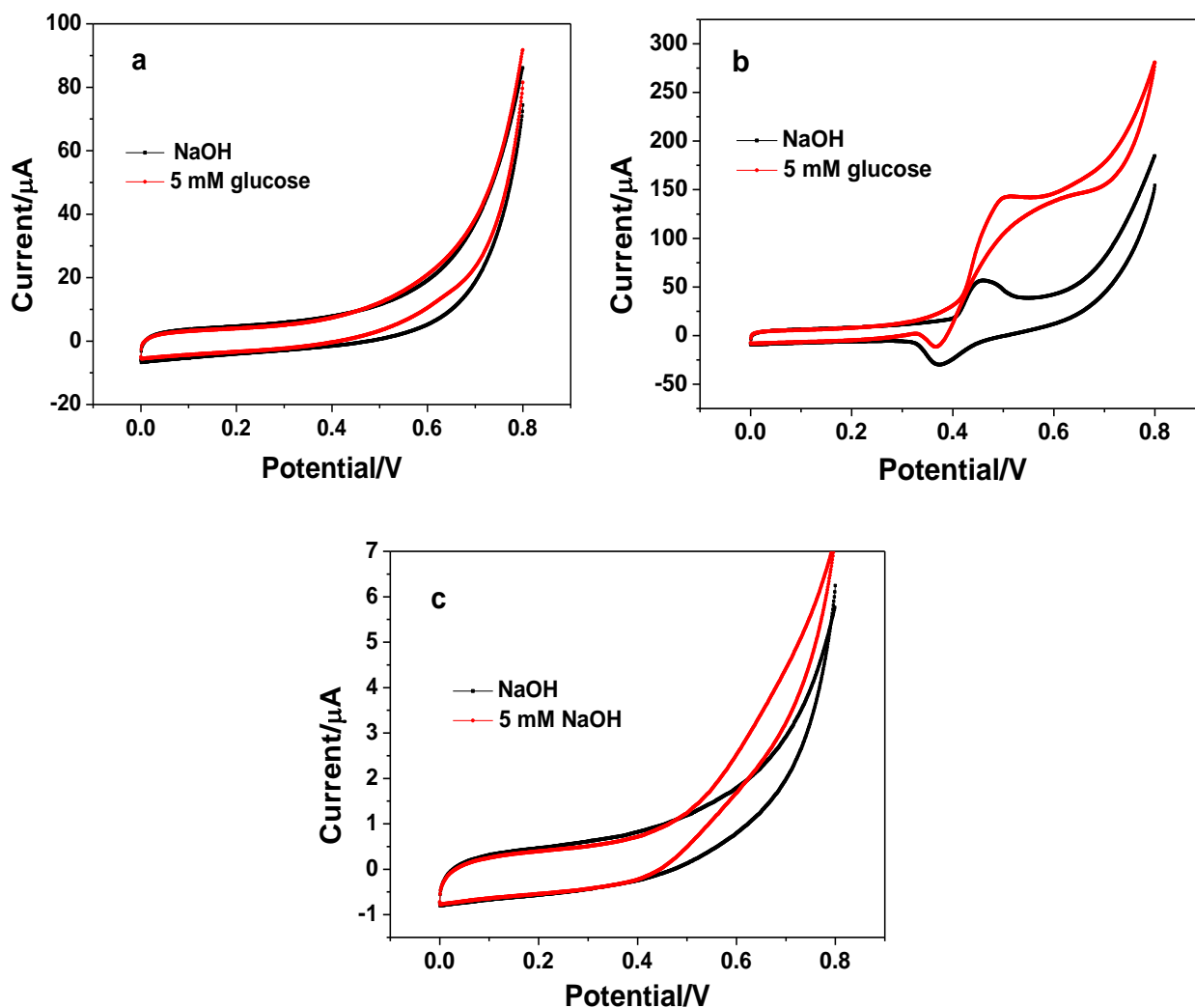


**Figure 6.** CV responses of RGO/GCE (a), NiOOH/RGO/GCE (b) and NiOOH/GCE (c) in 0.1 M NaOH solution without (black curve) and with 5 mM of glucose (red curve) involved at a scan rate of  $50 \text{ mV s}^{-1}$ .

Current-time curves were obtained to determine the amperometric sensing property of NiOOH/RGO nanocomposites electrode. Prior to amperometric detection of glucose, the influence of applied potentials was investigated. Fig. 7a exhibits amperometric response of NiOOH/RGO/GCE to successive additions of  $50 \text{ }\mu\text{M}$  glucose at different applied potentials. Obviously, the steady-state current response of  $50 \text{ }\mu\text{M}$  glucose increased notably from +0.3 V to +0.5 V. When the applied potential was further increased to +0.6 V, the current response of glucose is nearly comparable to that of +0.5 V, but the blank current was significantly enhanced compared to +0.5 V. Considering that the high applied potential will lead to poor selectivity because interference coexisting with glucose may be also oxidized at this potential. Hence, applied potential of +0.5 V was chosen.

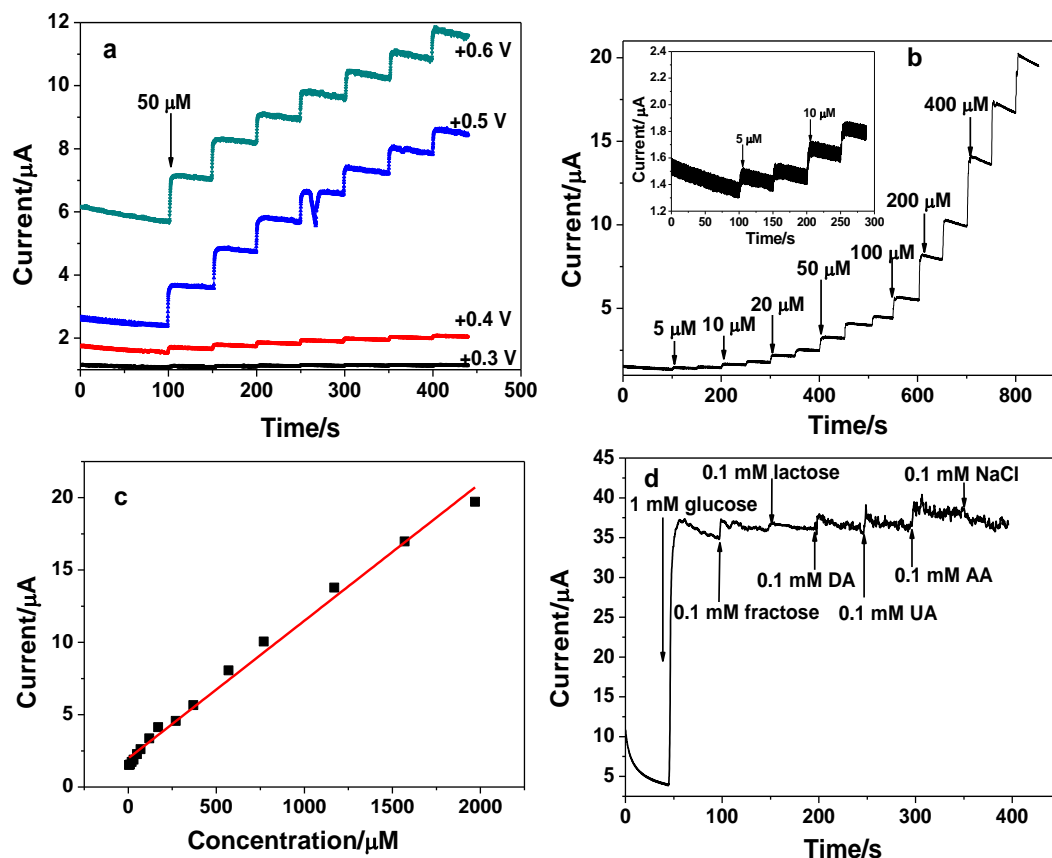


**Figure 7.** Detection of glucose in 0.1 M NaOH solution using the NiOOH/RGO/GCE: (a) Amperometric responses of NiOOH/RGO/GCE to successive additions of 50  $\mu\text{M}$  glucose at the applied potentials of +0.3, +0.4, +0.5 and +0.6 V, respectively; (b) Amperometric responses of the NiOOH/RGO/GCE (holding at +0.50 V) upon addition of glucose to increasing concentrations; (c) The relationship between current and glucose concentration with the data from Fig. 6b; (d) Amperometric responses of the NiOOH/RGO/GCE to successive additions of 1 mM glucose, 0.1 mM fructose, 0.1 mM lactose, 0.1 mM DA, 0.1 mM UA, 0.1 mM AA and 0.1 mM NaCl in 0.1 M NaOH at +0.5 V.

Fig. 7b displays the current-time curves of the NiOOH/RGO/GCE with successive additions of different concentrations of glucose in 0.1 M NaOH solution at an applied potential of +0.5 V. Obviously, the electrode shows rapid response to additions of glucose with a response time of  $<2$  s, revealing outstanding electrocatalytic performance of the NiOOH/RGO nanocomposites for oxidation of glucose. The amperometric responses to glucose present a good linear range from 5  $\mu\text{M}$  to 1.97 mM (as shown in Fig. 7c). The corresponding linear regression equation is written as  $I$  ( $\mu\text{A}$ ) =  $1.98168 + 0.0951C$  ( $\mu\text{M}$ ) with a correlation coefficient of 0.9960. From the equation, the detection limit and the sensitivity are estimated to be 1  $\mu\text{M}$  (signal-to-noise ratio of 3) and  $1346 \mu\text{A mM}^{-1} \text{cm}^{-2}$ , respectively. Comparison of the performance of the present NiOOH/RGO nanocomposites for non-enzymatic glucose sensing with those previously reported Ni-based materials was listed in Table 1. It is worth mentioning that the ultrathin NiOOH nanosheets on RGO surface exhibits comparable performance toward glucose in terms of the detection sensitivity, the linear range and detection limit. The prominent electrocatalytic behavior of the present NiOOH/RGO nanocomposites

should be ascribed to the following advantages: on the one hand, the large surface area of NiOOH nanosheets provide more active sites for electrocatalysis, and enhance the electroadsorption amount of glucose on electrode surface; on the other hand, the ultrathin structure facilitate transport of electron through the electrode-electrolyte interface; besides, the possible synergism occurred between NiOOH nanosheets and the highly conductive RGO material, enhanced the electrocatalytic activities of NiOOH nanosheets.

**Table 1.** Comparison of the performance of the present NiOOH/RGO nanocomposites for non-enzymatic glucose sensing with those previously reported Ni-based materials.

Electrode materials	Response time (s)	Sensitivity ( $\mu\text{A mM}^{-1} \text{cm}^{-2}$ )	Linear range	LOD ( $\mu\text{M}$ )	Ref
Ni(OH) <sub>2</sub> -HS	3	223.39	0.8749 $\mu\text{M}$ -7.781 mM	0.1	12
CS/ Ni(OH) <sub>2</sub> -NPs	-	72	0.5 mM-10 mM	-	19
RGO-Ni(OH) <sub>2</sub>	7	11.43	2 $\mu\text{M}$ -3.1 mM	0.6	23
Ni(OH) <sub>2</sub> @oPPyNW	10	1049	0.001 mM-3.86 mM	0.3	24
NiOHS <sub>s</sub> -RGO-NF	3	2721	0.6246 $\mu\text{M}$ -10.50 mM	0.03	29
Ni(OH) <sub>2</sub> /ERGO-MWNT	2	2042	10 $\mu\text{M}$ -1500 $\mu\text{M}$	2.7	30
NiO-SWCNTs	2	2980	0.5 $\mu\text{M}$ -1300 $\mu\text{M}$	0.056	34
Ni(OH) <sub>2</sub> -graphene	2	494	1 $\mu\text{M}$ -1000 $\mu\text{M}$	0.6	37
NiOOH/RGO	2	1346	5 $\mu\text{M}$ -1.97 mM	1	This work

Anti-interference property is a significant parameter for a desirable glucose biosensor. Some common substance coexisting with glucose in a biological sample, including fructose, lactose, dopamine (DA), uric acid (UA), ascorbic acid (AA) and NaCl often interfere with glucose signals. The concentration of interfering species is reported much lower than that of glucose in the human blood (4–7 mM) [38,39]. Thus, the effect of 0.1 mM interfering species on the amperometric response of 1 mM glucose was investigated to ensure the selectivity. From the current-time curve in Fig. 7d, a significant current was observed for glucose in comparison with the other six interfering species. All the interference yielded current response less than 7.2% compared to glucose. Therefore, the present NiOOH/RGO electrode was found to exhibit acceptable selectivity in the interference experiments conducted.

### 3.4. Electrocatalytic oxidation of GSH at the NiOOH/RGO nanocomposites electrode

GSH, an important thiol compound consisting in mammalian tissues, plays significant roles in most biological functions such as antioxidant defense, cell signaling and proliferation [40]. GSH is often electrochemically oxidized into glutathione disulfide (GSSG). The levels of GSH and the concentration ratio of GSH and GSSG indicate some oxidative stresses and cell functionalities. A large number of electrode materials, such as carbon [41-43] and metal based materials [2,44] have been employed for electrochemical quantification of GSH, but the cost-effective and easily available Ni

based materials is more prospective. Fig. 8a presents the CV responses recorded at  $50 \text{ mV s}^{-1}$  in the absence and presence of 5 mM GSH in 0.1 M NaOH. Upon addition of GSH, an increased anodic current with onset potential of +0.3 V corresponds to oxidation of GSH. This anodic peak current increased correspondingly with the increase of GSH concentration from 0 to 1 mM, as shown in Fig. 8b. For the application of amperometric determination at +0.6 V, a stable and fast response in current can be found (Fig. 8c) with the successive additions of different concentrations of GSH. The NiOOH/RGO electrode shows sensitive and fast amperometric response to GSH addition, obtaining steady-state current within 3 s. The plots of amperometric current vs GSH concentrations and corresponding calibration curve is showed in Fig. 8d. The response to GSH shows a good linear range from  $5 \mu\text{M}$  to  $770 \mu\text{M}$  (as shown in top left of inset of Fig. 8d).

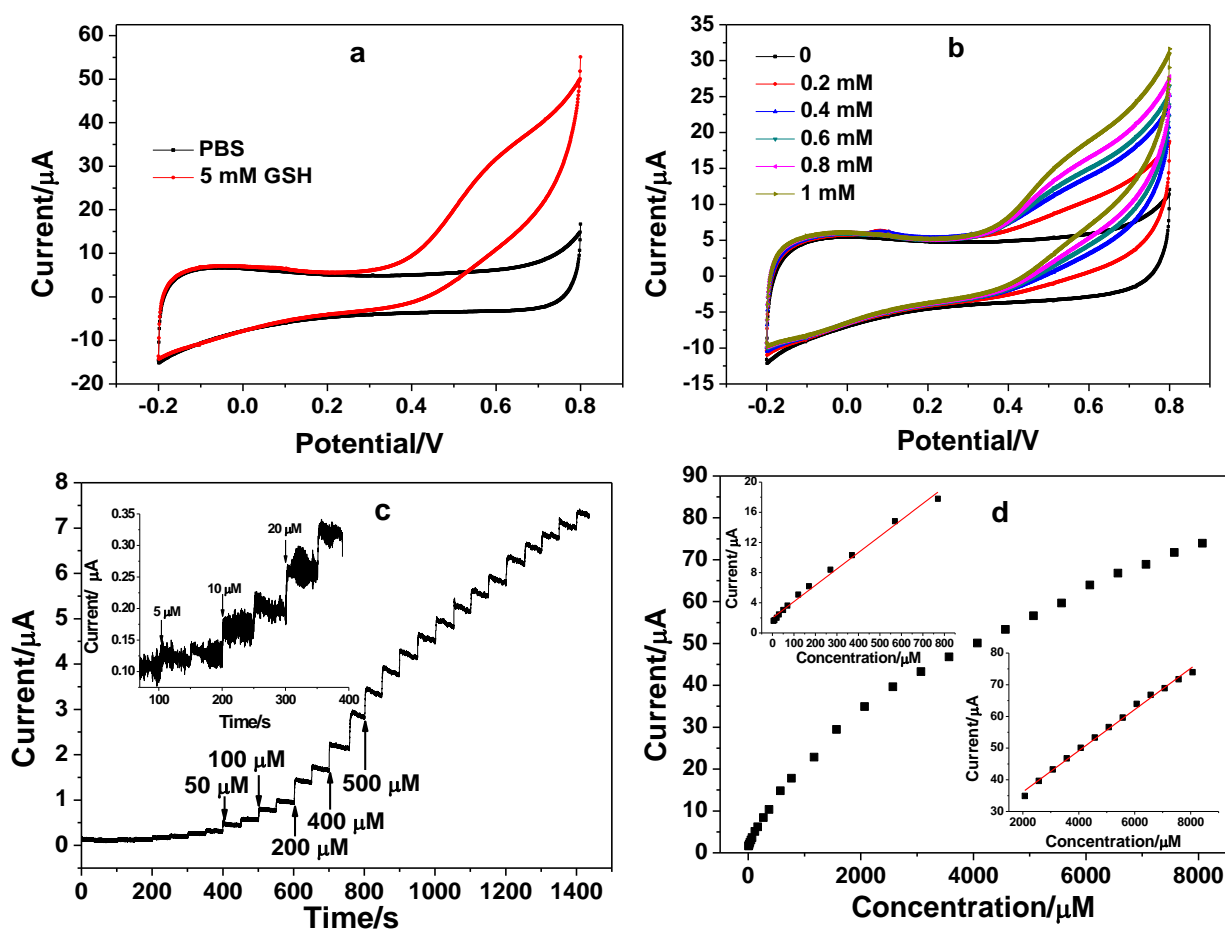


**Figure 8.** (a) CVs of NiOOH/RGO/GCE in 0.1 M NaOH with 5mM GSH involved (a) and with different concentrations of GSH (b) at a scan rate of  $50 \text{ mV s}^{-1}$ ; (c) Current-time responses of NiOOH/RGO/GCE upon addition of GSH to increasing concentrations at an applied potential of +0.6 V; (d) The plots of amperometric current vs GSH concentrations with the corresponding calibration curves in the inset.

The corresponding linear regression equation is written as  $I (\mu\text{A}) = 1.98809 + 0.02167C (\mu\text{M})$  with a correlation coefficient of 0.9954. The detection limit is estimated to be  $2 \mu\text{M}$ . The present linear range ( $5\text{--}770 \mu\text{M}$ ) is wider than that of  $3\text{--}130 \mu\text{M}$  obtained at ordered mesoporous carbon electrode

[45], 0.1–5.0  $\mu\text{M}$  at poly-m-aminophenol electrode [46], 4–28  $\mu\text{M}$  at ordered mesoporous carbon/cobalt oxide nanocomposite electrode [47], and is also comparable to some of previously reported electrochemical sensors [48,49]. When the concentration of GSH is above 770  $\mu\text{M}$ , the increase rate of amperometric responses with GSH concentration is found to lower, possibly due to the passivation of electrode surface caused by the adsorbed reaction intermediates. Meanwhile, the linear relationship (as shown in bottom right of inset of Fig. 8d) spans the concentration of glucose from 2.07 mM to 8.07 mM following a equation of  $I (\mu\text{A})=23.1759+0.0065C (\mu\text{M})$  ( $R=0.9974$ ). For the interference test, the results showed that 10  $\mu\text{M}$  glucose, 5  $\mu\text{M}$  UA, 5  $\mu\text{M}$  AA, 5  $\mu\text{M}$  DA, and 5  $\mu\text{M}$  glutathione disulfide did not interfere distinctly with the detection signal of 0.1 mM GSH. Therefore, the NiOOH/RGO electrode is a favorable electrocatalyst for GSH oxidation and shows potentials for monitoring GSH levels in biosensing applications.

### 3.5. Reproducibility and stability

To evaluate the reproducibility of the present electrodes, six NiOOH/RGO nanocomposites electrodes were prepared separately using the same procedures. The relative standard deviation (RSD) for current responses of 50  $\mu\text{M}$  glucose at +0.5 V and 50  $\mu\text{M}$  GSH at +0.60 V was 4.7% and 5.3% respectively, indicating a good inter-electrode reproducibility. In addition, seven measurements of 50  $\mu\text{M}$  glucose using the same electrode yielded a RSD of 3.4%, while for 50  $\mu\text{M}$  GSH, the RSD was only 2.9%. The long-term stability of developed electrode was evaluated by recording its current response every 3 days after placing it in air at room temperature for a period of time. It was found that the NiOOH/RGO nanocomposites electrode retained 90.8% of its original current response to 50  $\mu\text{M}$  glucose even after storage for 3 weeks, indicating good stability.

To verify the capability of the developed sensor in real sample analysis, the present method was used for the determination of glucose spiked in the human urine sample. The standard addition method was employed for obtaining the recovery test. The results are shown in Table 2. Obviously, acceptable recovery was found for sample 1 and sample 2, indicating that urine sample has no interference on direct analysis of glucose.

**Table 2.** Amperometric determination of glucose spiked in human urine samples (n=4).

Urine samples	Spiked ( $\mu\text{M}$ )	Found ( $\mu\text{M}$ )	R.S.D (%)	Recovery (%)
Sample 1	10.0	10.2	3.04	102
Sample 2	20.0	19.5	2.65	97.5

## 4. CONCLUSIONS

In summary, aqueous NiOOH with untrathin nanosheets structure were synthesized using a hydrothermal method and then it was modified on the RGO electrode surface through a self-assembly

method to form NiOOH/RGO nanocomposites. The electrocatalytic properties of the resultant NiOOH/RGO nanocomposites electrode toward small molecules of glucose and GSH were investigated. Thanks to the large surface area of NiOOH, its ultrathin nanosheets morphology and the possible synergism occurred between NiOOH nanosheets and the highly conductive RGO nanosheets, the as-prepared NiOOH/RGO nanocomposites electrode exhibited a high catalytic activity toward electrooxidation of glucose and GSH in alkaline conditions. As a potential electrochemical glucose and GSH sensor, the NiOOH/RGO electrode showed excellent performance including fast response, wide linear response range, high sensitivity and selectivity, and good reproducibility and stability. The present work sheds light on developing highly efficient and long-term stability electrocatalysts for glucose and GSH oxidation.

#### ACKNOWLEDGEMENTS

This work was supported by the Grants from the National Natural Science Foundation of China (21105002, 21273010), the fund project for Young Scholar sponsored by Henan province (13HASTIT014, 14HASTIT012, 2013GGJS-147) and for Henan Key Technologies R&D Program (122102310516, 12B150002).

#### References

1. S.J. Li, N. Xia, X.L. Lv, M.M. Zhao, B.Q. Yuan, H. Pang, *Sens. Actuators, B*, 190 (2014), 809.
2. B. Yuan, C. Xu, L. Liu, Q. Zhang, S. Ji, L. Pi, D. Zhang, Q. Huo, *Electrochim. Acta*, 104 (2013) 78.
3. A. Arabzadeh, A. Salimi, M. Ashrafi, S. Soltanian, *Catal. Sci. Technol.*, 6 (2016) 3485.
4. E. Katz, I. Willner and A. B. Kotlyar, *J. Electroanal. Chem.*, 479 (1999) 64.
5. D. Wu, D. Cheng, *Electrochim. Acta*, 180 (2015) 316.
6. S.M. El-Refaei, M.M. Saleh, M.I. Awad, *J. Power Sources*, 223 (2013) 125.
7. Y. Hu, Q. Shao, P. Wu, H. Zhang, C. Cai, *Electrochem. Commun.*, 18 (2012) 96.
8. K.C. Lin, Y.T. Hung, S.M. Chen, *RSC Adv.*, 5 (2015) 2806.
9. W. Li, R. Ouyang, W. Zhang, S. Zhou, Y. Yang, Y. Ji, Y. Yang, K. Feng, X. Liang, M. Xiao, Y. Miao, *Electrochim. Acta*, 188 (2016) 197.
10. J. Xu, J. Cai, J. Wang, L. Zhang, Y. Fan, N. Zhang, H. Zhou, D. Chen, Y. Zhong, H. Fan, H. Shao, J. Zhang, C. Cao, *Electrochem. Commun.*, 25 (2012) 119.
11. M. Baghayeri, A. Amiri, S. Farhadi, *Sens. Actuators, B*, 225 (2016) 354.
12. P. Lu, Q. Liu, Y. Xiong, Q. Wang, Y. Lei, S. Lu, L. Lu, L. Yao, *Electrochim. Acta*, 168 (2015) 148.
13. H. Liu, X. Wu, B. Yang, Z. Li, L. Lei, X. Zhang, *Electrochim. Acta*, 17 (2015) 745.
14. Y.S. Chen, J.H. Huang, *Biosens. Bioelectron.*, 26 (2010) 207.
15. M. Vidotti, S.I. Córdoba de Torresi, L.T. Kubota, *Sens. Actuators, B*, 135 (2008) 245.
16. A.R.T. Babaei, *Sens. Actuators, B*, 176 (2013) 543.
17. A. Gu, G. Wang, J. Gu, X. Zhang, B. Fang, *Electrochim. Acta*, 55 (2010) 7182.
18. J. Zolgharnein, E. Shariatmanesh, A. Babaei, *Sens. Actuators, B*, 186 (2013) 536.
19. A. Ciszewski, I. Stepniak, *Electrochim. Acta*, 111 (2013) 185.
20. K.O. Iwu, A. Lombardo, R. Sanz, S. Scirè, S. Mirabella, *Sens. Actuators, B*, 224 (2016) 764.
21. L. Wang, Y. Tang, L. Wang, H. Zhu, X. Meng, Y. Chen, Y. Sun, X.J. Yang, P. Wan, *J. Solid State Electrochem.*, 19 (2015) 851.
22. J. Liang, Y. Li, *Chem. Lett.*, 32 (2003) 1126.
23. Y. Zhang, F. Xu, Y. Sun, Y. Shi, Z. Wen, Z. Li, *J. Mater. Chem.*, 21 (2011) 16949.
24. J. Yang, M. Cho, C. Pang, Y. Lee, *Sens. Actuators, B*, 21 (2015) 93.
25. X. Li, S. Xiong, J. Li, J. Bai, Y. Qian, *J. Mater. Chem.*, 22 (2012) 14276.

26. D.B. Kuang, B.X. Lei, Y.P. Pan, X.Y. Yu, C.Y. Su, *J. Phys. Chem. C*, 113 (2009) 5508.
27. A.K. Geim, K.S. Novoselov, *Nat. Mater.*, 6 (2007) 183.
28. A.K. Geim, *Science*, 324 (2009) 1530.
29. P. Lu, J. Yu, Y. Lei, S. Lu, C. Wang, D. Liu, Q. Guo, *Sens. Actuators, B*, 208 (2015) 90.
30. W. Gao, W.W. Tjiu, J. Wei, T. Liu, *Talanta*, 120 (2014) 484.
31. H.L. Guo, X.F. Wang, Q.Y. Qian, F.B. Wang, X.H. Xia, *ACS Nano* 3 (2009) 2653.
32. S.J. Li, Y. Xing, G.F. Wang, *Microchim. Acta* 176 (2012) 163.
33. J. Yang, X. Liang, L. Cui, H. Liu, J. Xie, W. Liu, *Biosens. Bioelectron.*, 80 (2016) 171.
34. W. Yi, D. Yang, H. Chen, P. Liu, J. Tan, H. Li, *J. Solid State Electrochem.*, 18 (2014) 899.
35. M. Jafarian, F. Forouzandeh, I. Danaee, F. Gobal, M.G. Mahjani, *J. Solid State Electrochem.*, 13 (2009) 1171.
36. F. Wolfart, A. Maciel, N. Nagata, M. Vidotti, *J. Solid State Electrochem.*, 17 (2013) 1333.
37. N.Q. Qiao, J.B. Zheng, *Microchim. Acta*, 177 (2012) 103.
38. S.J. Li, J.M. Du, J. Chen, N.N. Mao, M.J. Zhang, H. Pang, *J. Solid State Electrochem.*, 18 (2014) 1049.
39. S.J. Li, N. Xia, X.L. Lv, M.M. Zhao, B.Q. Yuan, H. Pang, *Sens. Actuators, B*, 190 (2014) 809.
40. X. Zhao, S. Zhou, Q. Shen, L.P. Jiang, J.J. Zhu, *Analyst*, 137 (2012) 3697.
41. Y. Hou, J.C. Ndamanisha, L.P. Guo, X.J. Peng, J. Bai, *Electrochim. Acta*, 54 (2009) 6166.
42. J.C. Ndamanisha, J. Bai, B. Qi, L.P. Guo, *Anal. Biochem.*, 386 (2009) 79.
43. R.R. Moore, C.E. Banks, R.G. Compton, *Analyst*, 129 (2004) 755.
44. M. Wen, H.Q. Liu, F. Zhang, Y.Z. Zhu, D. Liu, Y. Tian, Q.S. Wu, *Chem. Commun.*, 2009 4530-4532.
45. J.C. Ndamanisha, J. Bai, B. Qi, L.P. Guo, *Anal. Biochem.*, 386 (2009) 79.
46. Y. Oztekin, A. Ramanaviciene, A. Ramanavicius, *Electroanalysis*, 23 (2011) 701.
47. Y. Hou, J.C. Ndamanisha, L.P. Guo, X.J. Peng, J. Bai, *Electrochim. Acta*, 54 (2009) 6166.
48. F. Xu, L. Wang, M.N. Gao, L.T. Jin, J.Y. Jin, *Anal. Bioanal. Chem.*, 372 (2002) 791.
49. X.J. Wang, X. Chen, D.G. Evans, W.S. Yang, *Sens. Actuators, B*, 160 (2011) 1444.